Puzzle cell shape emerges from the interaction of growth with mechanical constraints

Nicola Trozzi[1,2], Brendan Lane[1], Alice Perruchoud[2], Yixuan Wang[2], Lukas Hörmayer[2], Mylan Ansel[3], Corentin Mollier[3], Alice Malivert[3], Frances Clark[4], Tammo Reichgelt[5], Adrienne H.K. Roeder[4], Olivier Hamant[3], Arezki Boudaoud[6], Dorota Kwiatkowska[7], Adam Runions[8], Richard S. Smith[1*✉] and Mateusz Majda[1,2✉]

[1]Department of Computational and Systems Biology, John Innes Centre, Norwich NR4 7UH, UK.

[2]Department of Plant Molecular Biology, University of Lausanne, CH-1015 Lausanne, Switzerland.

[3]Laboratoire de Reproduction et Développement des Plantes, Université de Lyon, ENS de Lyon, UCBL, INRAE, CNRS, 69364 Lyon Cedex 07, France.

[4]Weill Institute for Cell and Molecular Biology and School of Integrative Plant Science, Section of Plant Biology, Cornell University, Ithaca, NY 14853, USA.

[5]Department of Earth Sciences, University of Connecticut, Beach Hall, 354 Mansfield Rd, Storrs CT 06269, USA.

[6]LadHyX, Ecole polytechnique, CNRS, IP Paris, 91128 Palaiseau Cedex, France.

[7]Institute of Biology, Biotechnology and Environmental Protection, Faculty of Natural Sciences, University of Silesia, 40-032 Katowice, Poland.

[8]Department of Computer Science, University of Calgary, Calgary, AB T2N 1N4, Canada.

✉To whom correspondence may be addressed: Mateusz.Majda@unil.ch, Richard.Smith@jic.ac.uk.

Abstract

The puzzle-shaped cells found in the shoot epidermis of many plant species are a fascinating example of complex cell shapes. Because biological form often follows function, the unique shape of these cells suggests that they must serve some adaptive purpose for the plant. We previously proposed that these intricate shapes provide an effective strategy for reducing mechanical stress on the cell wall when epidermal cells undergo growth in more than one direction. Here we analyze a large selection of living and paleo plant species and find that the ability to make puzzle cells is a shared feature across all plant species, although their presence can be hidden as it varies depending on the organ, developmental stage, and environmental conditions. Computational modeling of *Arabidopsis* and maize epidermal cells revealed that presence and patterning of lobes is a dynamic process that is intricately linked to the growth history and environmental context of the plant organ. Conversely, disrupted lobeyness in mutants or with drug treatments affects plant development and leads to compensatory strategies. We propose that the mechanism underlying the formation of puzzle-shaped cells is likely conserved among higher plants and is a response to a developmental constraint driven by growth and mechanical stress.

Keywords: mechanical stress, growth, cell shape, pavement cells, puzzle cells

Introduction

Plant cells are tightly connected to their neighbors, and their growth must be coordinated to maintain tissue and organ integrity. This coordination is achieved through cell wall synthesis and remodeling, which is tightly connected with oriented divisions and controlled expansion of individual cells, resulting in a variety of cell shapes (Hulskamp *et al.,* 1998). For example, rod-shaped cells in roots or hypocotyls elongate along the apical-basal axis, while in flat and broad leaves they grow in multiple directions to form more diverse shapes

(Gendreau *et al.,* 1997; Sapala *et al.,* 2018). Epidermal pavement cells, which often develop jigsaw puzzle shapes, serve as an example of multipolar growth. Though pavement cells display local anisotropy and variation in anisotropic growth at the subcellular scale, these cells are commonly found in aerial organs with relatively more isotropic shapes (Sapala *et al.,* 2018, Zuch *et al.,* 2022).

Turgor pressure, which induces tensile stress on the walls, is essential for maintaining the shape of green plant tissue, and its removal leads to wilting. To withstand this pressure, the cell walls must be strong, yet they also need to extend to accommodate growth. We previously proposed that puzzle cells are formed to reduce stress in the cell wall when cells become large (Sapala *et al.,* 2018). The puzzle-shaped cells are essential for expansion of organs likes leaves, which grow in more than one direction. Without the puzzle shape, large endoreduplicated cells would bulge excessively and experience significant stress. The size of the Largest Empty Circle (LEC) that fits inside a cell in the paradermal plane can serve as a proxy for this stress (**Figure 1T**) (Sapala *et al.,* 2018). Puzzle shapes enable cells to grow large without increasing the LEC. Therefore, the intricate geometries of puzzle shapes limit the local turgor-induced stress on the cell wall as they grow, developing lobes to reduce the LEC. This mechanism not only provides a potential fitness benefit but also represents a response to a developmental constraint imposed by the physics of plant cell and tissue structure.

At the subcellular scale, cortical microtubules play a role in directing cellulose synthases, which extrude newly synthesized cellulose microfibrils to stabilize the pattern of cortical microtubules (Baskin, 2005). In pavement cells, cellulose microfibrils accumulate in the neck regions of a cell, acting to restrict growth and enable the formation of lobes (Panteris and Galatis, 2005, Panteris, 1994). Lobe formation occurs through stiffening of indented sides, aligning with cellulose and pectin patterns in the cell wall, which might be preceded by cell wall mechanical buckling (Bidhendi *et al.,* 2019). The distribution of stress patterns has been proposed to direct the orientation of microtubules (Hejnowicz *et al.,* 2000), which in turn direct cellulose microfibrils to reinforce the lobe areas, leading to the hypothesis that puzzle shapes emerge via a mechanical feedback loop (Sampathkumar *et al.,* 2014). Sapala *et al.* (2018) demonstrated that this mechanism can reproduce the wide variety of pavement cell shapes observed in plants. This idea is attractive since a stress-based mechanism would be a natural choice for limiting stress in the cell. Although a molecular mechanism to directly measure stress is not known, the Sapala *et al.* (2018) model uses geometry for feedback, suggesting that the curvature of the cell could serve as a proxy for stress. The model provides an important insight, that puzzle cell shape emerges from the interaction of the growth restrictions with cell expansion, resulting in cell shapes that reflect the growth history of the tissue.

Here we demonstrate that the mechanism for creating puzzle shapes is likely conserved in higher plants, although it may not always be evident. This formation is a dynamic process sensitive to developmental stages, specific organs, and environmental contexts. Importantly, these variations can be linked to the growth dynamics following cell division, where alterations in cellular growth rates and directions play a crucial role. Using computational modeling, we show how these post-division growth dynamics directly impact the emergence of puzzle-shaped cells. For example, in time-lapse observations on maize, we observed that changes in growth anisotropy over time correspond with the development of these complex cell shapes. This under-

scores that the formation of puzzle-shaped cells is not just a static feature, but a dynamic response to growth conditions.

Results

Why doesn't lobeyness always correlate with cell size?

In Sapala *et al.* (2018) we proposed lobeyness as a measure of the puzzle shape, which is defined as the ratio of a cell's perimeter to the perimeter of its convex hull (the inverse of convexity) (**Figure 1T**). This measure slightly improves upon another frequently used measure of lobes, solidity, which is the area of the cell over the area of the convex hull. With our measure of lobeyness, long thin cells with gentle curves that do not have lobes (*i.e.*, boomerang shaped) do not receive as high scores as they would when measured with solidity. Creating lobes enables cells to increase in size without the large empty circle (LEC) becoming too large. Sapala *et al.* (2018) found a positive correlation between cell area and lobeyness in *Arabidopsis* cotyledons and in most leaves from the 19 plant species they examined. Vofely *et al.* (2018) reported that they did not see a similar correlation in their data; however, they used the average solidity and area per species, and looked for the correlation across species, rather than looking at correlations in individual species as was done in Sapala *et al.* (2018). Furthermore, a correlation between lobeyness and cell area would not be expected in elongated cells, as they can have a large area without increasing their LEC. To address this problem, we propose that the minor axis (min axis), which refers to the length of the shorter of the two cell axes, serves as a better measure for capturing the aspect of cell size that is relevant for stress (**Figure 1T**). In order for the cell to have a large min axis, it must be large in both the major and min axes.

The ability to form puzzle shapes is not limited to leaves

The plasticity of epidermal pavement cells, both in their morphogenesis and response to environmental factors, raises the question of how many plant species are able to form puzzle cells, even if they do not display this feature in leaves grown in a particular environment. To address this question, we examined the shapes of epidermal pavement cells in various plant organs, including leaves, petals, sepals, and fruits. In certain species, such as linden (eudicot, *Tilia cordata*, **Figure 1A-F**) or crownvetch (eudicot, *Securigera varia*, **Suppl. Figure 1A, B**), the epidermal pavement cells in leaves are non-lobed. This observation prompted us to investigate whether the mechanism for creating lobed cells is present in the plant but not expressed in leaves. Our findings revealed that despite the absence of lobes in leaves, they do appear in other organs, such as bracts in linden (**Figure 1D-F**) or petals in crownvetch (**Suppl. Figure 1B**). In linden, it was surprising as the bracts have elongated organ shapes, whereas the leaves are rounder. This phenomenon proved to be more widespread than we initially thought, occurring in numerous other species, including cemetery iris (monocot, *Iris albicans*), spring crocus (monocot, *Crocus vernus*), and sepals in St John's wort (eudicot, *Hypericum perforatum*), common gorse (eudicot, *Ulex europaeus*) and blackthorn (eudicot, *Prunus spinosa*), where non-lobed epidermal pavement cells are found in leaves, but lobed cells are present in the epidermis of other organs (**Suppl. Figure 1C-L**). This suggests that these plants can develop lobed cells, although the lobing phenomenon does not manifest in leaves, and thus would be missed in any assay looking only at leaves (Vofely *et al.*, 2019).

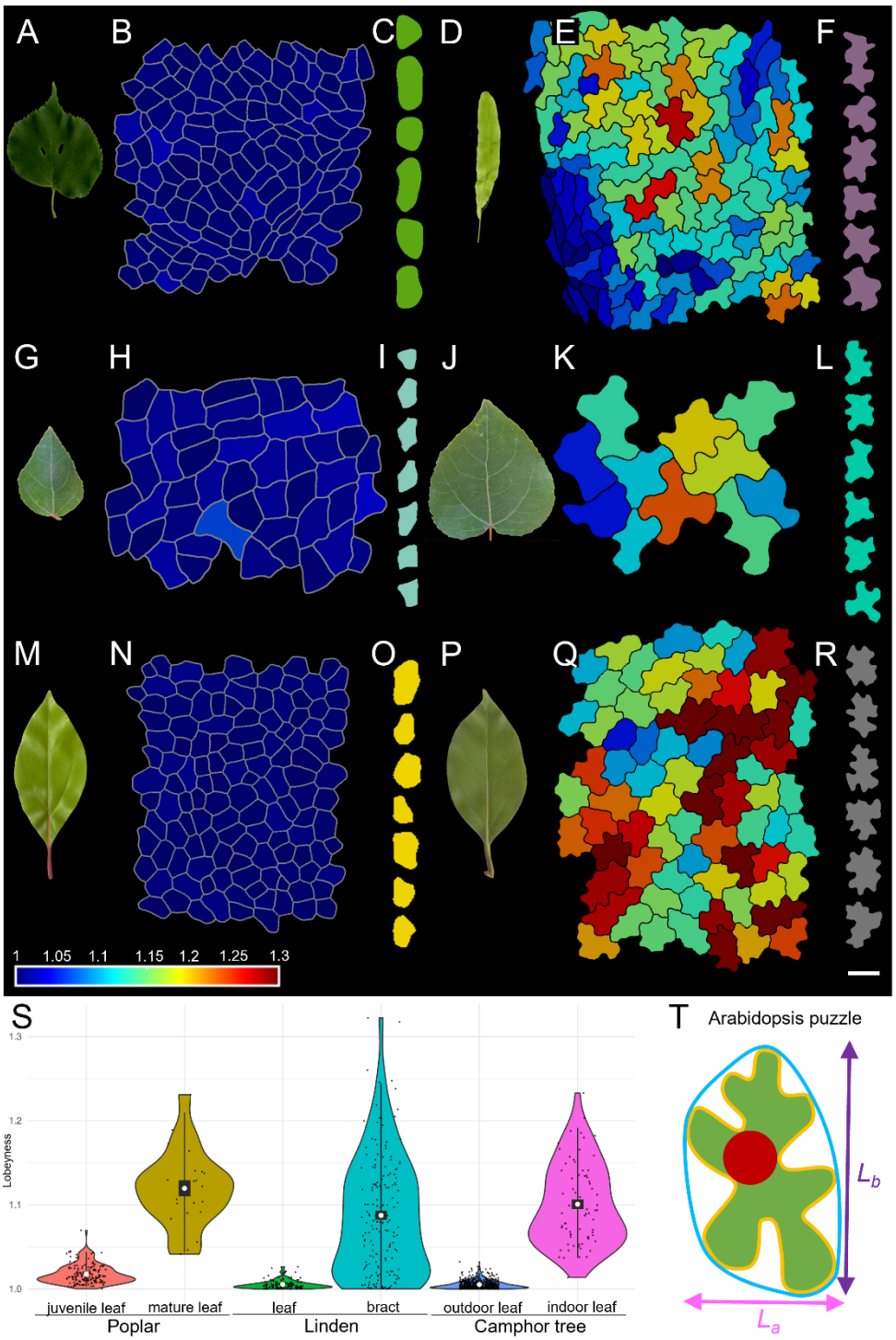

Figure 1. Pavement cell shapes demonstrate high plasticity, are regulated by development and environment, and vary among different organs. Images depict organ shapes (**A, D, G, J, M, P**), lobeyness heatmaps for epidermal pavement cell contours (**B, E, H, K, N, Q**), and cell outlines near the 95th percentile of lobeyness (**C, F, I, L, O, R**). Representative epidermal cell outlines from linden (*Tilia cordata*) are shown for leaves (**A-C**) and bracts (**D-F**). The adaxial sides of young (**G-I**) and fully developed (**J-L**) poplar tree leaves (*Populus tremula*). Representative epidermal cell outlines from camphor tree (*Cinnamomum camphora*) leaves grown outdoors (**M-O**) and indoors (**P-R**). The violin plot displays the distribution of lobeyness values in pavement cells across the conditions and organs represented in (**A-R**). Within the violin plot, the median is marked by a white circle, the interquartile range is indicated by a grey box, and 1.5 times the interquartile range is represented by grey lines (**S**). The visual depiction of the pavement cell descriptors: area is shown in green, lobeyness is defined as the perimeter of a convex hull (blue) divided by the cell perimeter (yellow), the minor axis (L_a) is represented by the length of the shorter axis (in contrast to the major axis L_b), and the large open area (LEC) representing the magnitude of mechanical stress (red) (**T**). Scale bar: (**K, Q**) 10 µm, (**H**) 15 µm, (**C, I, L, O**) 20 µm, (**N, R**) 25 µm, (**B**) 40 µm, (**E, F**) 50 µm.

Pavement cell shape reflects the environmental context of the plant

To compare cell shape in different organs and among individuals growing in varying conditions, we performed an analysis of epidermal pavement cells collected from different contexts. To explore whether the degree of lobeyness could be influenced by variations in developmental stage, we compared the epidermal pavement cell outlines among leaves at different stages of growth within the same plant. We observed that young (not fully developed) leaves were less lobed than larger, mature leaves in several species, such as quaking aspen (eudicot, *Populus tremuloides)* (**Figure 1G-L**), lilac (eudicot, *Syringa vulgaris*, **Suppl. Figure 1M, N**), and camphor tree (eudicot, *Cinnamomum camphora*, **Suppl. Figure 1O, P**). Interestingly, in some cases, such as lilac, cells previously reported as non-lobed (Vofely *et al.* 2019) appeared lobed in our data set, likely due to developmental stage. Fully developed lilac leaves revealed the presence of puzzle-shaped cells, although their expression was not always pronounced. However, the onset of puzzle-shape formation varied among different species, suggesting that plants that can form puzzle-shaped cells may not do so until later in development. Furthermore, variations in pavement cell shape were also observed between two sides of the same leaf – abaxial and adaxial. This phenomenon was evident in the leaves of love-lies-bleeding (eudicot, *Amaranthus caudatus*) (**Suppl. Figure 2A-C**), Peruvian-lily (eudicot, *Alstroemeria aurea*) (**Suppl. Figure 2D-F**), fuchsia (eudicot, *Fuchsia magellanica*) (**Suppl. Figure 2G-I**), peppermint (eudicot, *Mentha x piperita*) (**Suppl. Figure 2J-L**), and cigar flower (eudicot, *Cuphea ignea*) (**Suppl. Figure 2M-O**). In these species, the abaxial (lower) side of the leaves tended to exhibit more lobed shapes compared to the adaxial (upper) side, which is directly exposed to sunlight (Watson, 1942). Similarly, environmentally controlled plasticity of pavement cells was observed in fully developed epidermal cells of camphor tree. While this species typically displays non-lobed pavement cells (Zhao *et al.,* 2006), we found that when grown in a greenhouse, the pavement cells exhibited puzzle shapes, whereas this morphology was not observed when plants were cultivated outdoors (**Figures 1M-R**). This observation is consistent with the idea that making puzzle shapes is an actionable mechanism to adapt to the environment, and not only a passive consequence of the environment such as sun exposure or humidity. Our study is in line with the usage of degree of sinuosity in paleoecology to distinguish sun leaves from shade leaves (Kürschner, 1997; Bush *et al.,* 2017). Additionally, these observations indicate that the program that shapes pavement cells to produce lobes can be activated late in the individual leaf development, even in leaves that have cells that are typically non-lobed.

We analyzed the epidermal pavement cells in fully developed leaves of 3-week-old *Arabidopsis thaliana* (**Figure 2A**), quantified their cell area (**Figure 2B**), min axis (**Figure 2C**) and lobeyness (**Figure 2D**). When correlating lobeyness with their min axis, we found a stronger positive correlation than with cell area (**Figure 2E, F**). To assess the prevalence of these correlations, we conducted a large-scale analysis of lobeyness, and min axis across 327 species and 663 species-organ combinations, totaling over 72,026 cells. In our analysis, we collected new samples from 45 species in various plant organs and incorporated data from previously published analysis of leaf epidermal pavement cells in 19 species from Sapala *et al.* (2018), 250 species from Vofely *et al.* (2018), and data from 45 leaves of 13 early Miocene species (**Suppl. Table 1**) (Reichgelt *et al.,* 2020). The plotted relationship between min axis and lobeyness showed a moderate or higher positive correlation (≥ 0.3) in the majority of species (235 out of 327, 72%) (**Figure 2G**). Some species display particularly high correlations, such as a correlation coefficient (Corr) of 0.97 for tobacco (eudicot, *Nicotiana tabacum*), 0.94 for the lacy tree fern (fern, *Sphaeropteris cooperi*) and 0.91 for morning glory (eudicot, *Ipomea tricolor*) (**Suppl. Figure 3A-C**).

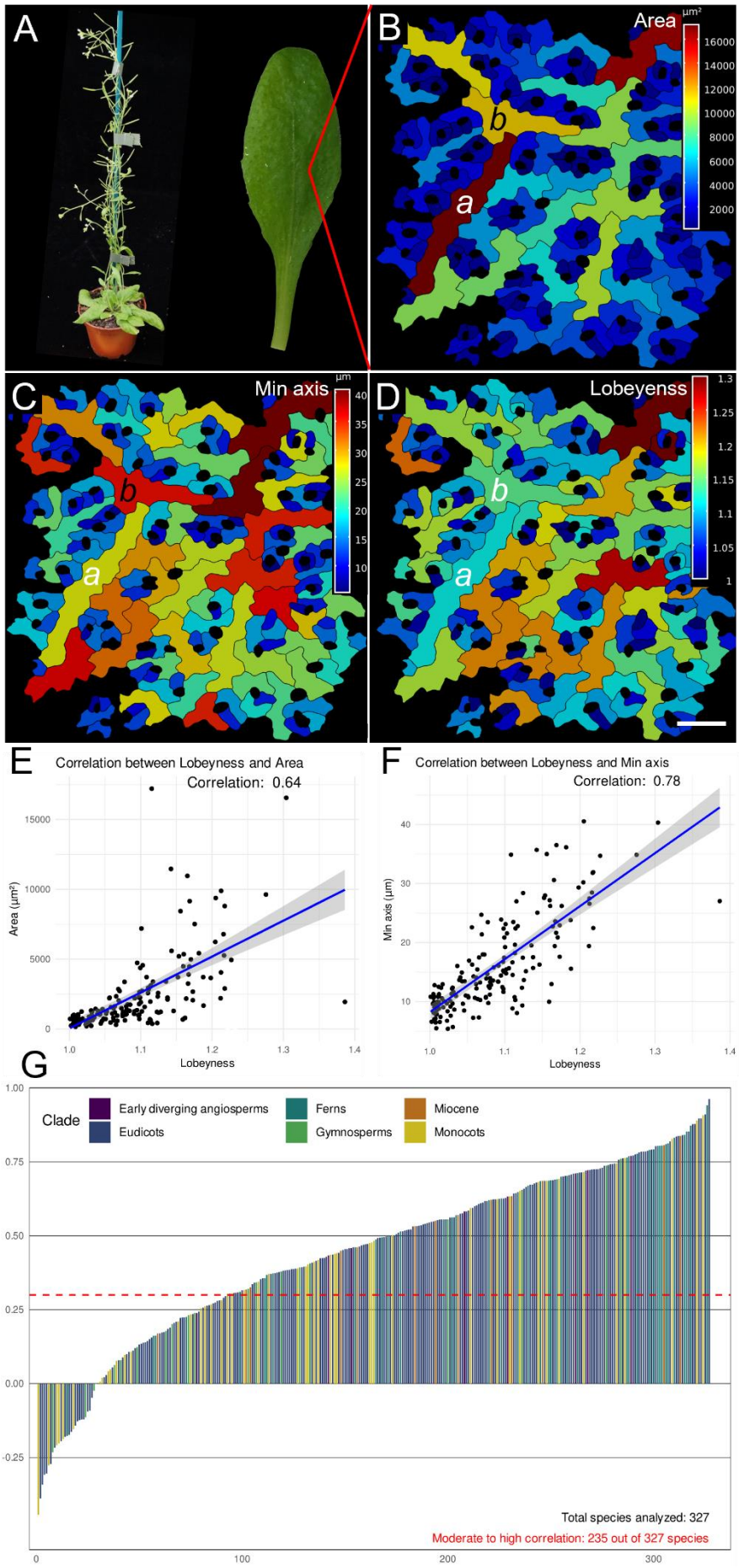

Figure 2. Lobeyness appears widely as a response to increasing cell size. An image representing the region of interest of a fully developed 3-week-old leaf of *Arabidopsis thaliana* wild type (**A**). The confocal images of epidermal pavement cells were acquired using propidium iodide staining for cell wall visualization, and the images were segmented in MorphoGraphX to visualize different parameters (**B-D**). Epidermal cell templates representing cells colored by area (**B**), min axis (**C**), and lobeyness (**D**). Graphs presenting the correlation between area and lobeyness (Corr = 0.64) (**E**) and between min axis and lobeyness (**F**). The correlation between min axis and lobeyness in leaf epidermal pavement cells across 327 species (**G**). A bar plot graph displaying each species represented as a single bar, color-coded by clade. The colors corresponding to each clade are shown in the figure. A dashed red line setting at a value of 0.3, which indicates the threshold for medium-high correlation. Most species exhibit a significant positive correlation (**G**). Scale bars: 100 µm (**B-D**).

However, some species exhibited weak or even negative correlations between the min axis and lobeyness (**Figure 2H, Suppl. Figure 3D-I**), which seems contradictory to the notion that stress serves as a developmental constraint. Upon further examination of these cases, we identified several reasons for lack of a strong correlation in certain samples. In cardboard palm (gymnosperm, *Zamia furfuracea*) growth is highly anisotropic, resulting in elongated cells where the min axis does not increase with cell length (**Figure 3B**). In this case lobes are not expected to be formed. Another example is the leaf of yellow guava (eudicot, *Psidium guajava*) where cells continue dividing to maintain a uniform size and a low min axis, even though the leaves can become quite large (**Figure 3C**). Cells can sometimes exhibit only a weak correlation if there is limited variability in the min axis or lobeyness, as observed in the samples with non-lobey small cells in pinwheel flower (eudicot, *Tabernaemontana divaricata*) (**Figure 3D**) or highly lobey cells in hare's foot fern (fern, *Davallia solida*) (**Figure 3E**). In some species that do not make lobes, staggering cells with neighbors affects the thinner elongated cells to a greater extent, as seen in blue lily (monocot, *Agapanthus praecox*) (**Figure 3F**), while in Virginia spiderwort (monocot, *Tradescantia virginiana*), the irregular shape of smaller stomatal lineage cells leads to higher lobeyness scores (**Figure 3G**).

Beyond the average: most epidermal cells are able to make jigsaw puzzle shapes

There are several strategies that plants can use to maintain low levels of LEC to minimize stress on the cell wall. They can continue dividing to keep the LEC small, induce anisotropic expansion to form thin elongated cells or display localized cell expansion to form puzzle-shaped cells. Multiple strategies can often co-exist within a single plant or even within the same organ. For example, both strategies are observed in pavement cells in the leaf of elderberry (eudicot, *Sambucus nigra*) (**Suppl. Figure 4A, B**) and in bracts of linden (eudicot, *Tilia cordata*) (**Suppl. Figure 4C, D**). In those species, small cells associated with the stomatal lineages do not make lobes, cells above vascular tissues are elongated, and cells above the mesophyll are lobey. In many instances, the median or mean cell shape may not exhibit significant lobeyness, even though the plant has the capacity to generate lobed cells. Calculating an average shape in such cases does not accurately reflect the plant's ability to make puzzle shaped cells. To determine a plant species' ability to develop lobed cells, a more reliable measure is to compare the presence or absence of lobed cells among the analyzed species, preferably sampling as many organs and developmental contexts as possible. For this purpose, we selected the 95th percentile of cell lobeyness to represent a species' ability to make puzzle-shaped cells. This enabled us to determine whether a species can make lobed cells or not, rather than averaging the shape from leaves consisting of a mosaic of cells at different developmental stages (Majda *et al.,* 2017; Elsner *et al.,* 2018). For better visualization, we displayed a single pavement cell showcasing the 95th percentile of lobeyness for each analysed species (**Figure 3H**). Our analysis demonstrated that most species we examined have the ability to generate lobed cells, even if the average cell shape for many of these species does not exhibit significant lobeyness as reported by Vofely *et al.* (2019) (**Figure 3I**).

Figure 3 (→ next page). Lobeyness is a common feature observed across different species. Cell contours of leaves color-coded by clade (**A-G**). An example of a high correlation between min axis and lobeyness in the pavement cells of tobacco (*Nicotiana tabacum*) (Corr = 0.97) (**A**). A lack of correlation typical for long and thin cells in the carboard palm (*Zamia furfuracea*) (Corr = 0.24) (**B**). Epidermal cells in the yellow guava (*Psidium guajava*) maintain small cells of a uniform size (Corr = 0.38) (**C**). A lack of correlation observed in the epidermis with little variation in cell size in the pinwheel flower (*Tabernaemontana divaricata*) (Corr = 0.13) (**D**). Highly lobey

cells in the hare's foot fern (*Davallia solida*) display little variation in lobeyness, which influences the correlation (Corr = 0.16) (**E**). Small cells from the stomatal lineages in the agapanthus (*Agapanthus praecox*) display concave indentations resulting in negative correlations (Corr = -0.21) (**F**). Negative correlations typical for pavement cells in the Virginia spiderwort (*Tradescantia virginiana*) with stomatal lineage cells displaying irregular concave shapes (Corr = -0.2) (**G**). A visual representation of a single pavement cell from each analyzed species, showing the 95th percentile of lobeyness (**H**). Bar plot of the 95th percentile of lobeyness values (**I**). The color-coding by clade is displayed on the figure. Scale bars: (**E**) 100 µm, (**A-D**, **F**) 200 µm, (**G**) 250 µm, (**H**) 500 µm.

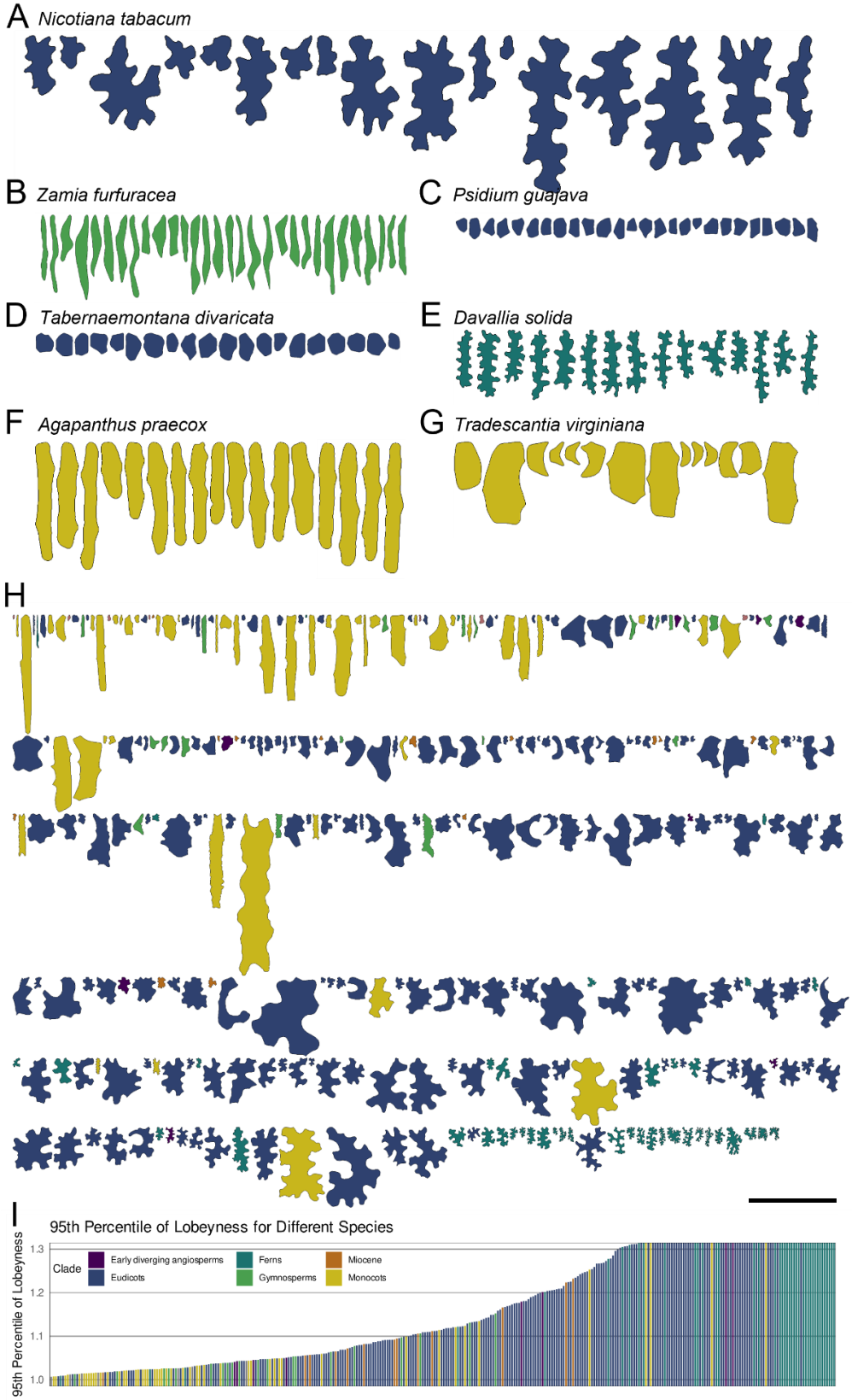

Puzzle shapes limit the LEC as cell size increases

Our hypothesis suggests that as cell area increases, further increases in LEC will be inhibited. Consequently, compared to small cells, large cells are expected to exhibit a smaller increase in LEC for the same increase in area. This behaviour can be assessed using a quadratic fit line passing through the origin (**Suppl. Figure 5A**), which our hypothesis predicts would curve to the right ($\alpha < 0$). Consistent with our hypothesis, we observed LEC area increases more slowly than cell area (**Suppl. Figure 5B, C**). The slower increase of LEC compared to area has consequences for cell shape. Namely, cells must exhibit a tendency towards becoming either elongated or lobed (or snake-like), as otherwise LEC would increase in proportion to area. To assess what happens to cell shape in the case when cells must expand in more than one direction, we can use the min axis. Here we also observe that LEC area increases more slowly than the min axis (**Suppl. Figure 5D, E**), consistent with increases in LEC being supressed as cell size increases. Examining this tendency at the clade (**Suppl. Figure 5F-K**) and species level shows that this relationship is pervasive. Overall, we observe negative α values in 87% of all species (286 of 386 species, $p < 2e^{-16} < 0.05$, exact binomial test). This behaviour is consistent with clade level observations (exact binomial test is used for the following p-values). As we are examining how LEC increases with respect to min axis length, elongated cells do not suffice to explain this relation. Instead, cells must have a tendency to become more lobed (or snake-like). The supports our hypothesis that the puzzle cell shape works to limit the size of the LEC, and the stress on the wall.

Pavement cell shape reflects the growth history of the organ

Our model (Sapala *et al.,* 2018) operates based on the growth restrictions (springs) placed across the cell, mimicking the role of microtubules in directing downstream cellulose deposition. In this mechanism, small indentations attract connections, while the protrusions lose them, causing the lobes and indentations to be enhanced. Consequently, regions that are enriched in connections experience restrictions while regions devoid of connections bulge outwards. To evaluate how our model behaves on actual epidermal cell shapes, we visualized cell walls and cortical MT distribution (**Figure 4A**). We then segmented cells to obtain templates for the model. By simulating the distribution of connections using these templates, we observed that the arrangement of connections quantitatively resembles the pattern of cortical microtubules (**Figure 4B**). Notably, both connections and cortical microtubules accumulate in the indentations, while they are absent in the lobes, aligning with the predictions of our model. We previously demonstrated in our simulation model that the appearance of puzzle cells depended on the nature of the growth field Sapala *et al.* (2018). Counter-intuitively, we found that isotropic growth at the tissue scale led to complex shapes, whereas strongly anisotropic growth at the tissue scale led to elongated cells with a simpler shape. This suggests that it might be possible to infer the growth history of a plant organ by examining the shape of its epidermal cells. Because Sapala *et al.* (2018) model did not account for changes in growth pattern over time, here we conducted computational simulations to investigate how the distribution of growth over time affects cell shape. Initially, our model consisted of isodiametric cells (**Figure 4C**), and we explored the impact of varying growth rates in the x and y directions on individual cell shapes. The initial and final templates were of the same size, with only the growth function varying. Thus, total growth was the same, although its dynamics changed over time. We adjusted the total growth so that the template expanded twice as much in the y direction than the x direction. Our findings revealed several intriguing patterns. When the growth rate remained uniform and

constant over time, puzzle-shaped cells similar to those observed in *Arabidopsis thaliana* formed (**Figure 4D**), even with the 2:1 anisotropy. On the other hand, when growth was initially isotropic but later switched to anisotropic growth (with increased growth in the y direction), the cells adopted a distinct elongated shape with lobes (**Figure 4E**). Conversely, when anisotropic growth was followed by isotropic growth, cells became elongated without lobes (**Figure 4F**). These results demonstrate that changes in growth rate and direction over time have a significant impact on cell shape, even if the total growth is the same.

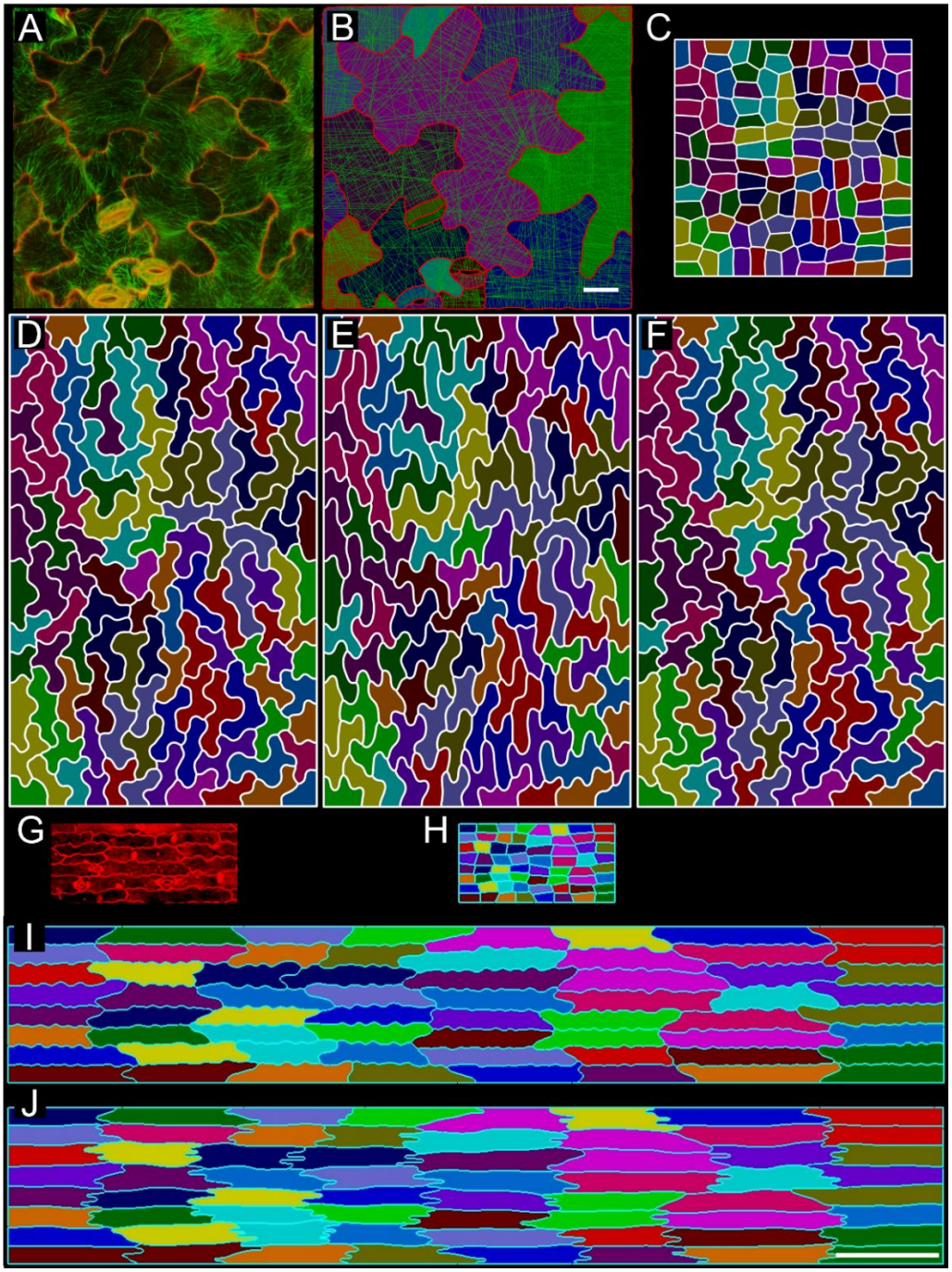

Figure 4. Growth distribution over time influences the shapes of pavement cells. Confocal image representing epidermal pavement cells from a fully developed 3-week-old leaf of *Arabidopsis thaliana*. The cell wall was visualized using propidium iodide staining (red), and the microtubules were visualized using fluorescent TUA6-CFP (green) (**A**). A visualization of the placement of connections across the cells for these shapes in the computational model (**B**). Model simulation across various growth fields (**C-F**). The initial template (**C**) for the shapes evolved over 300 growth iterations into the final state, which is 16 times larger in the y direction and 10 times larger in the x direction (**D-F**). Uniform anisotropic growth with puzzle-shaped cells; growth rates in the x and y directions are different but

constant over time (**D**). Separate periods of isotropic growth and maximally anisotropic growth in only the y direction (**E, F**). Isotropic growth (250 steps) followed by anisotropic growth (50 steps) resulting in puzzle-shaped cells whose lobes are largely oriented vertically (**E**). Anisotropic growth (50 steps) followed by isotropic growth (250 steps) resulting in with a less pronounced, but still noticeable, horizontal orientation (**F**). (**G-J**) Cell shape in Zea Maize. Typical cell shapes in maize leaves (**G**). Initial starting template representing unexpanded cells (**H**). Cell shapes after growth in the model is set to that observed experimentally (**I**). The effect on cell shape when the template is first grown in width, then in length, to reach the same final template size and shape (**J**).Scale bars: (**A**-**B**) 20 µm, (C-F) arbitrary units, (**H-J**) 200 µm.

To validate the predictions of our model, we performed time-lapse experiments on maize (*Zea mays*). The epidermal cells of maize are elongated but exhibit a puzzle-like shape that emerges in cells located at a specific distance from an intercalary meristem. To capture the morphogenesis of maize pavement cells, we obtained sequential replicas of cell patches on the surface of juvenile leaves. These patches were located at various distances from the intercalary meristem allowing us to reconstruct the entire process of cell development using only two consecutive time points. These observations suggest that the shape of maize puzzle cells arises from an initial period of strongly anisotropic growth followed by a less anisotropic phase (**Suppl. Figure 6**). Initially, maize leaves experienced strong anisotropic growth, primarily in the longitudinal direction. As development progressed, elongation decreased while growth in the transverse direction remained nearly constant, leading to decrease of anisotropy. At this stage the lobe morphogenesis begins (**Figure 4G**). To simulate the development of maize cell shapes, we initialized the simulation on the model template with a representative geometry of cells (**Figure 4H**). We adjusted the growth rates and anisotropy, taking into account their changes over the time as observed in the time-lapse data. This enabled us to accurately reproduce the shape of the maize puzzle cells and the timing of their emergence (**Figure 4I**). We then perturbed the model by imposing a period of growth that was first in width followed by a period of growth in the longitudinal direction to achieve the same final template. This results in cell shapes substantially different to those observed (**Figure 4J**). These findings highlight the significance of growth dynamics, including changes in growth rates and anisotropy, in shaping the characteristics puzzle cell shape.

Physiological relevance of the ability to make puzzle shapes epidermal cells

Our model so far shows that plant adjust their pavement cell shapes to their environment and growth history. Conversely, is such adaptation critical for plant development? In particular, as epidermal growth is generally through to act as a limiting factor for plant development (Kutshera and Niklas 2007). We disrupted lobeyness through genetic and pharmacological approaches. We examined the leaf epidermal pavement cells in various mutants that display defects in puzzle cell shape acquisition. Compared to the *Arabidopsis thaliana* wild type (**Figure 5A, Suppl. Figure 7A**), the *constitutively active Rho-of-Plants (ROP) 2 (CA-ROP2)* mutant display altered accumulation of actin filaments (AFs) in the lobes resulting in non-lobed pavement cells (Fu *et al.,* 2002). Our analysis showed that lobeyness in *CA-ROP2* was completely abolished, but the lack of lobes was partially compensated by the presence of elongated and snaky cells (**Figure 5B, Suppl. Figure 7B**). We also analyzed *anisotropy1 (any1),* which carries the D604N missense primary cell wall cellulose synthase A1 (CesA1) mutation affecting crystalline cellulose synthesis (Fujita *et al.,* 2013). Similar to the previous mutant, the lack of lobes in *any1* was partially compensated by the presence of sinuous cells (**Figure 5C, Suppl. Figure 7C**). The *constitutive triple response (ctr1)* mutant, a negative regulator of ethylene signaling, showed reduced lobeyness, partially compensated by an increase in division activity with majority of small cells (**Figure 5D, Suppl. Figure 7D**). This observation prompted us to analyze if lobeyness is correlated with

division activity. We quantified the epidermal cells in leaves of LOSS OF GIANT CELLS FROM ORGANS (LGO), which is controlling the endoreduplication in plants (Schwarz and Roeder 2016). In comparison to the wild type with proper pavement cell shapes (**Suppl. Figure 8A**), the *lgo-2* mutant, which does not undergo the endoreduplication displayed increased division activity with many small cells with fewer lobes (**Suppl. Figure 8B**), while LGO OX line displayed giant pavement cells with highly undulated outlines (**Suppl. Figure 8C**). This observation indicates that increased cell division activity leads to less lobey cells, as small cells with low LEC are not expected to lobe (**Suppl. Figure 8D**). Compared to the wild type, all the mutants displaying altered lobeyness and LEC (**Figure 5I**) exhibited smaller leaf sizes, and plants showed reduced growth or were dwarfed (**Figure 5E-H**). These observations indicate that the absence of lobed cells hampers cell expansion and has a notable impact on overall plant growth.

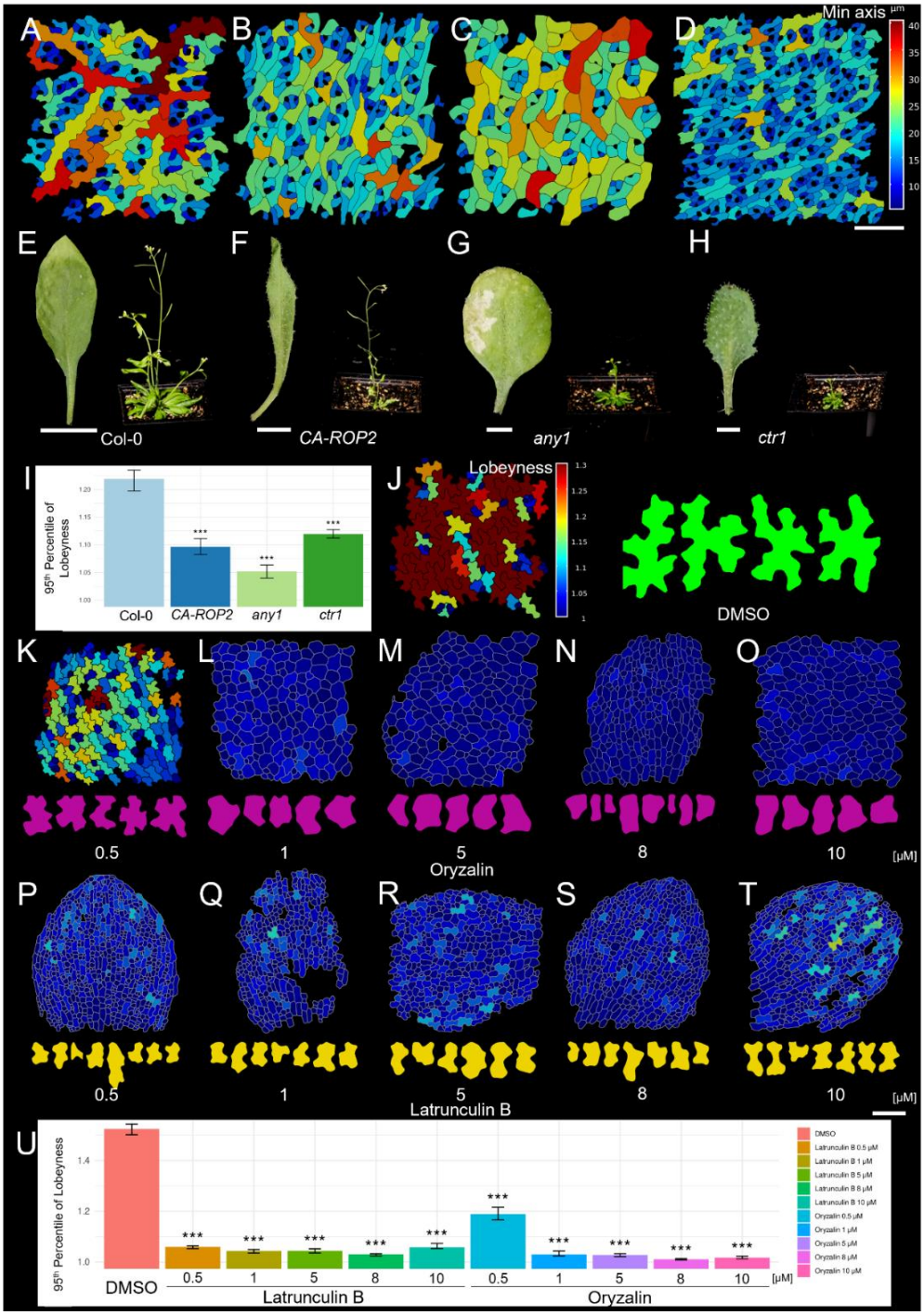

Figure 5: The lack of lobes is associated with overall growth defects. The shape of epidermal pavement cells (**A-D**) and overall growth phenotypes (**E-H**) in 3-week-old *Arabidopsis thaliana* wild type and mutants. Puzzle cells in the wild type displaying high lobeyness (**A, E**). Thin and elongated epidermal pavement cells in the *CA-ROP2* mutant displaying decreased lobeyness (**B**), with long and thin leaves, and reduced overall plant growth (**F**). Snaky epidermal pavement cells in the *any1* mutant displaying decreased lobeyness (**C**), with smaller and round leaves, and plants displaying dwarf phenotypes (**G**). Small epidermal pavement cells in the *ctr1* mutant displaying decreased lobeyness (**D**), with very small leaves, and plants displaying dwarf phenotypes (**H**). The bar plot of the 95th percentile of lobeyness for different mutants, with statistical significance of these values determined using bootstrapping; significance is marked by asterisks and standard error (**I**). The effect of pharmacological treatments on the shape of epidermal pavement cells (**J-U**). The mock treatment retains the typical morphology of puzzle cells (**J**). Dose-dependent oryzalin treatments result in a gradual decrease in lobeyness and an increase in LEC (cells labelled in violet) (**K-O**). Dose-dependent latrunculin B treatments lead to a decrease in lobeyness with shallow lobes (cells labelled in yellow) (**P-T**). These treatments are administered in increasing concentrations of 0.5, 1, 5, 8, and 10 µM. The 95th percentile of lobeyness bar plot for drug treatments, with statistical significance of these values determined using bootstrapping; significance is marked by asterisks and standard error (**U**). Scale bars: (contours **J-T**) 50 µm, (epidermis **J-T**) 100 µm, (**A-D**) 200 µm, (**H**) 1 mm, (**G**) 2 mm, (**F**) 5 mm, (**E**) 50 mm.

We attempted to confirm the genetic result with an independent approach. We performed pharmacological treatments of cotyledons using oryzalin and latrunculin B. By employing dose and time-dependent treatments, we were able to control and regulate the inhibitory effects of these drugs. Oryzalin, a substance that depolymerizes MTs, was used to disrupt the MT accumulation that creates the future neck regions of puzzle cells, by impairing the growth restrictions in these zones. Latrunculin B treatment blocks actin polymerization, which along with microtubules, has been proposed to play a critical role in pavement cell morphogenesis (Panteris and Galatis 2005). Additionally, actin filaments play an important role in delivery of the polysaccharides to the wall matrix. Thus, inhibition of actin filaments could have an effect in localized delivery of pectin homogalacturonan to the wall, which are crucial in early stages of lobes formation (Bidhendi *et al.,* 2019). Strikingly, all the treated plants exhibited reduced cotyledon sizes and overall inhibited plant growth, similar to the observed phenotypes in the mutants. The observed reductions in cotyledon size and overall plant growth further highlight the significance of the ability to make puzzle shape cells in promoting normal plant development. Compared to control samples (**Figure 5J**), low doses of oryzalin resulted in cells with wider neck regions and larger LECs, indicating a decreased accumulation of MTs (**Figure 5K, L**). Increasing the dose of oryzalin led to a decrease in lobeyness (**Figure 5M, N**), and at very high concentrations, puzzle cell formation was completely abolished, resulting in nearly isodiametric shapes (**Figure 5O**). In contrast, latrunculin B treatment affected the depth of lobe formation and reduced lobeyness (**Figure 5P-T**). Notably, even at high doses, latrunculin B did not completely eliminate lobe formation, unlike the oryzalin treatment (**Figure 5U**). This suggests that MT-driven local restrictions on growth are more critical for acquiring the puzzle cell shape.

Alternative strategies to compensate for the lack of lobes in epidermal cells

So far, our results show that plants make jigsaw puzzle shapes in response to their environment and organ growth, and we provide evidence that this mechanism affects plant growth in a feedback loop (Sampathkumar *et al.,* 2014). Yet, pavement cells lacking the typical puzzle-like shape do not undergo rupture or cell death. This suggests two possibilities: either these cells experience low mechanical stress or they employ alternative mechanisms to compensate for their non-ideal geometry. We propose two hypotheses to explain this resilience: an increase in cell wall stiffness, which could be achieved through either thickening of the cell wall or alterations in its composition, thereby changing its mechanical properties; or a reduction in turgor

pressure within the cell. To test the first hypothesis regarding cell wall stiffness, we conducted osmotic treatments on cotyledons subjected to varying doses of oryzalin (**Suppl. Figure 9**). After transferring the plants from water to a sorbitol solution to eliminate the tensile stress exerted by turgor on the walls, we observed contraction (**Figure 6A-F**), allowing us to approximate cell wall elasticity. Contrary to expectations, we found that higher oryzalin concentrations correlated with greater cell shrinkage: 10.4% at 0 µM to 16.7% at 2 µM (**Figure 6I**). This suggests that oryzalin exposure softens, rather than stiffens, the cell walls. This softening effect of oryzalin on cell walls is consistent with the idea that cellulose microfibrils, which overlay microtubules, accumulate in the LEC regions (Sampathkumar *et al.,* 2014). This may contribute to the altered mechanical properties of the cell wall, explaining why these cells do not resort to stiffening as a compensatory mechanism. This also aligns with prior research in the shoot meristem of *Arabidopsis* showing that cells with disrupted microtubules—like those exposed to oryzalin—fail to stiffen their walls effectively, leading to cell rupture (Sapala *et al.* 2018).

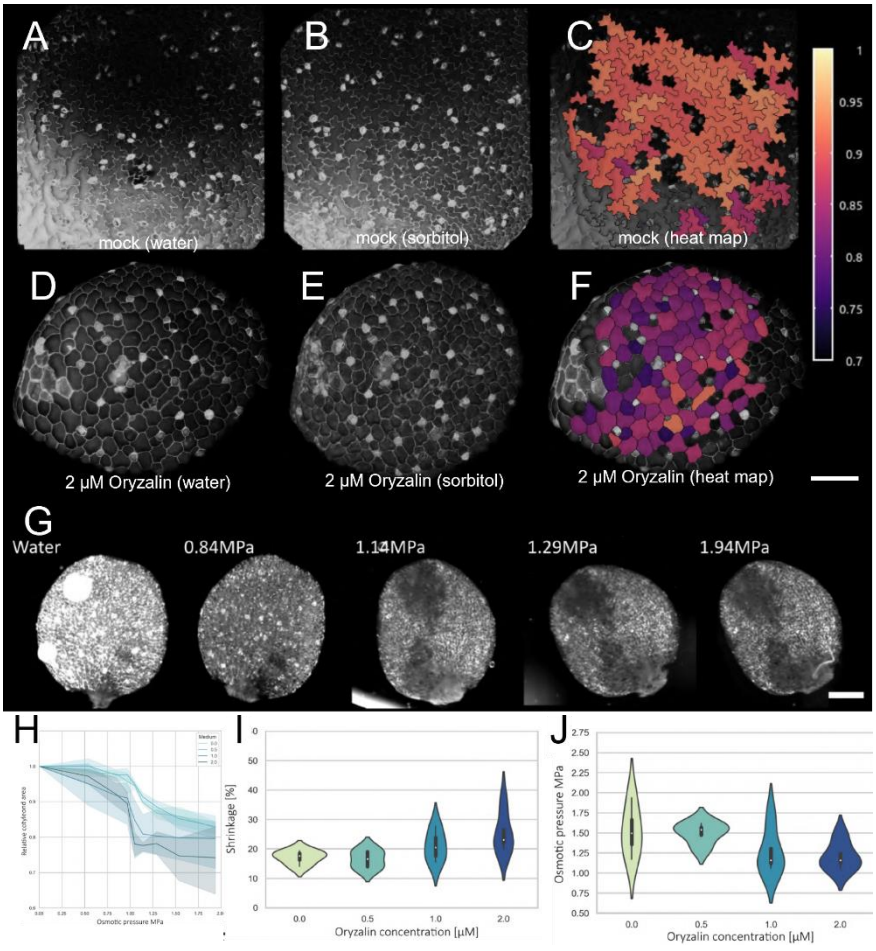

Figure 6. Cells compensate the lack of lobes by forming more elastic walls. Osmotic treatments to study the effect of cell geometry change on cell wall elasticity (**A-F**). Confocal images of epidermal pavement cells in cotyledons grown on the control medium (**A-C**), and medium supplemented with oryzalin leading to non-lobey cells (**D-F**). Individual samples were imaged in water (**A, D**) and sorbitol causing the cell wall to shrink (**B, E**), and the heatmaps presenting the amount of shrinking were generated (1 = no deformation) (**C, F**). Representative images of cotyledons in the wild type imaged after 15 minutes at different NaCl treatments (**G**). Relative cotyledon areas for mock treatment and different oryzalin concentrations imaged at different osmotic pressure conditions (**H**). Shrinkage of cotyledons observed at different oryzalin concentrations, which informs about the wall elasticity (n=4) (**I**). Osmotic pressure corresponding to the inflection point measured at different oryzalin concentrations (n=4) (**J**).

To explore the second hypothesis whether the loss of puzzle shape affects turgor pressure, we used a plasmolysis assay to gauge the average turgor pressure in cotyledons. We measured the cotyledon area at 15-minute intervals in solutions of increasing NaCl concentrations. The osmotic pressure for each solution (0, 0.54, 0.84, 0.97, 1.05, 1.14, 1.29, 1.54, and 1.94 MPa) was calculated based on osmolarity measurements (**Figure 6G**). The osmotic pressure at the highest NaCl concentrations is elevated. This could be due to cellular osmoregulation, where cells adjust ion concentrations to maintain osmotic balance, or the influence of guard cells, which control stomata and respond to osmotic changes. By dividing the cotyledon area in each

solution by the area in the solution without NaCl, we obtained the relative cotyledon area as a function of the osmotic pressure (**Figure 6H**). We measured the shrinkage of the cotyledons, defined as the relative cotyledon area in the last NaCl solution. We observed a correlation between oryzalin concentration and increased cotyledon shrinkage, from 18% at 0µM to 23% at 2µM (**Figure 6I**). This trend aligns with our previous measurements, although the values are about 40% higher. To obtain relative indications of turgor pressure in cotyledons we considered that as the osmotic pressure in the medium increases, turgor pressure decreases (Beauzamy *et al.,* 2014). Therefore, a lower osmotic pressure at the inflection point, defined as the osmotic pressure at which the curve changes its direction from shrinking to stabilizing, indicates a lower turgor pressure. We observed that the inflection point was reached at a lower osmotic pressure as the concentration of oryzalin increased, from 1.49 MPa at 0µM to 1.16 MPa at 2µM (**Figure 6J**). Notably, instead of flattening out at zero pressure, the curves show a sudden drop. We attribute this drop to a simultaneous bursting of multiple cells, especially evident under higher oryzalin concentrations where the cell walls are softer, leading to visible damage on the cotyledons. This analysis opens the path for the analysis of the relation between pavement cell shape and hydraulics.

Discussion

In our previous work, we proposed that the primary purpose of the puzzle cell shape is to prevent epidermal cells from developing large open areas that would bulge out under turgor pressure, leading to considerable stress (Sapala *et al.,* 2018). This suggests that the puzzle cell shape is a response to a physical constraint shared by all plants. However, not all plants exhibit puzzle cells Vofely *et al.* (2019), and there are several reasons for this, related to the various options available to plants in dealing with this constraint. One option is for cells to continue division, as observed in leaves of some plant species such yellow guava (*Psidium guajava*). However, in many plant species, there is a transition from dividing, meristematic cells to larger cells that undergo endoreduplication as they expand and become very large (**Suppl. Figure 8**). This process is common in epidermis of various plant organs, including leaves, roots and sepals of *Arabidopsis*. In roots and sepals of *Arabidopsis*, growth is highly anisotropic resulting in large but elongated cells. In such cases, the puzzle shape is unnecessary (from the structural point of view), as there are no large open areas, and the cell shape remains simple. This represents another option, where long, thin cells can become very large without increasing stress. In situations where growth is not strictly anisotropic, such as in the leaves and cotyledons of *Arabidopsis*, larger cells adopt the puzzle shape to mitigate bulging and stress. This is essential because, under these conditions, a lack of puzzle-shaped cells would lead to the formation of large, open areas subject to considerable turgor pressure, thereby placing the cell walls under significant stress. Another option to manage stress in large, isodiametric cells would be to develop a very thick cell wall. However, this mechanism is not commonly observed, likely because it would require substantial resources to maintain.

According to our hypothesis, the puzzle shape is required in the epidermis of all plant organs that contain large cells with isotropic growth (*i.e.,* not limited to the formation of long and thin cells). Previous research by Sapala *el al.* (2018) found a correlation between cell lobeyness and cell area. In contrast, Vofely *et al.* (2019) did not observe this correlation. In our study, we merged the data from these previous studies, and augmented it with additional species, including plant organs beyond leaves, such as sepals, bracts, and some species from the fossil record (Reichgelt *et al.,* 2020). This comprehensive analysis revealed that while some

species may not exhibit puzzle cells in their leaves, they might still develop puzzle cells in other organs like sepals or bracts. Additionally, we discovered that the appearance of puzzle cells can be influenced by the developmental stage of the plant and environmental conditions. Our analyses indicate that most higher plants are able to make puzzle cells. While Vofely *et al.* (2019) reported that the average shape of plant cells is "weakly undulated", we were interested in determining whether or not the plant has the mechanism to make puzzle cells. To address this question, we examined the 95th percentile of lobeyness in each species across all sampled organs. Our analysis showed that most species do contain cells that exhibit a significant puzzle cell shape (**Figure 3H, I**), and those that do not tend to either have elongated cells (**Figure 3B**) or keep dividing (**Figure 3C, Suppl. Figure 8B**).

Since stress on the cell wall is a mechanical constraint, the mechanism of generating puzzle cells is likely widely conserved, even if the trait is not always displayed. The presence or absence of puzzle cells in different contexts within the same species likely reflects differences in growth patterns rather than variations in the underlying puzzle shape patterning mechanism. The differences in growth, such as growth amounts, timing, or anisotropy may even determine whether puzzle cells appear or not. This makes it challenging to isolate the mechanism of puzzle cell formation from the broader regulation of growth. Any gene that controls growth amounts, timing or anisotropy may alter the observed puzzle cell phenotype, even if it is not involved in the mechanism that controls the patterning. Thus, phylogenetic analysis and screens for puzzle cell shape formation are likely to conflate genes involved in growth regulation with those governing the mechanism of lobe formation. These approaches can inadvertently capture genes that influence growth or cell division, even if they are not directly involved in the mechanism underlying lobe formation. This inherent connection between growth regulation and puzzle cell formation poses a challenge in dissecting the specific mechanisms responsible for shaping puzzle cells and untangle the interplay between growth regulation and the underlying patterning mechanisms.

Puzzle cell shape is tightly coupled with growth, as it is isotropic growth at the tissue level that leads to lobe formation at the cell level. In contrast, strongly anisotropic growth, such as in roots or stems, results in elongated cells with simple shapes. Our analysis of epidermal pavement cells in maize leaf demonstrated that the cell shape it produces arises from initially strong anisotropic growth that gradually becomes less anisotropic over time. Interestingly, when different growth dynamics were applied to the same initial template in our model, it produced different cell shapes. This highlights the dependence of puzzle cell formation on specific growth patterns that can evolve over time. It raises the fascinating question of how much information about the growth history can be extracted from the shapes of puzzle cells themselves. Notably, in tissues characterized by highly lobed cells, such as *Arabidopsis* leaves, it becomes evident that significant isotropic (*i.e.*, similar in all directions) growth must have occurred since the cells stopped dividing. As pavement cell shape can be considered as a proxy of growth history and environmental conditions, they can now be revisited in plant fossils too. This is reminiscent of the analysis of leaf shapes at a larger scale, and the presence of lobed leaves resulting from their packing in buds, thus acting as a proxy for temperate climates (Couturier 2009). Through our analysis of mutants and pharmacological treatments, we showed that certain plants can partially compensate for the loss of puzzle cell formation by generating snaky cells that intertwine. However, the overall trend in these plants suggests that complete disruption of the puzzle cell mechanism leads to dwarf-

ism, as the cells are unable to expand fully. Taken together our findings strongly suggest that puzzle cells form in response to a mechanical constraint, and the underlying mechanism is likely highly conserved among higher plants.

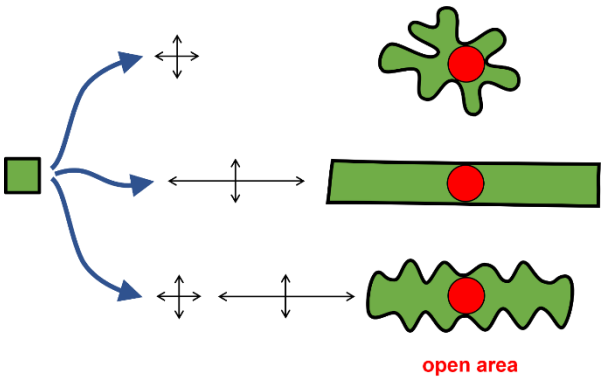

Figure 7. Graphical abstract illustrating how the puzzle cell shape emerges from the interaction of growth with mechanical constraints. Uniform growth yields a puzzle-shaped cell, while anisotropic growth results in an elongated cell. A combination of both uniform and anisotropic growth produces a cell with mixed characteristics—both elongated and with lobes. Throughout these growth patterns, the LEC, represented by a red circle, remains consistently small, highlighting the cell's strategy to maintain a compact LEC regardless of growth direction.

Material and Methods:

Plant material and growth conditions

The seeds were sterilized by immersing them in a solution of 70% EtOH (Sigma-Aldrich, Cat: 64-17-5) and TWEEN® 20 (Sigma-Aldrich, Cat: P9416) for 2 minutes. Subsequently, they were rinsed twice with 95% EtOH and left to air dry. The sterilized seeds were then placed in square Petri plates (Sigma-Aldrich, Cat: Z692344) filled halfway with a growth medium composed of ½ MS (Murashige and Skoog Basal Salt Mixture, Duchefa Biochemie, Cat: M5524), 1% sucrose (Fisher, Cat: 57-50-1), at pH 5.6, and 0.7% agar (Duchefa Biochemie, Cat: P1001). After a period of 72 hours of stratification at 4°C, the seeds were grown in a vertical position for 5 days at 22°C, with a 16-hour light cycle per day, in a controlled environment room. Subsequently, the 5-day-old seedlings were transferred to soil and cultivated for 4 weeks at 22°C, with a 16-hour light cycle per day. The screen of epidermal pavement cell outlines was conducted on *Arabidopsis thaliana* Col-0 ecotype and the following lines: *anisotropy1* (*any1*) (Fujita *et al.,* 2013), *constitutively active GTP-bound rop2* (*CA-ROP2*) (Li *et al.,* 2001), and *constitutive triple response1* (*ctr1*) (Kieber *et al.,* 1993). For the microtubule imaging, seeds of green fluorescent protein – α-TUBULIN6 (GFP-TUA6) line (Ueda *et al.,* 1999) were grown on a Petri plate for 12 days and stained with 0.1% PI prior imaging. For the cell wall elasticity and turgor pressure measurements, pAR169 (pATML1::mCitrine-RCI2A) line was used to visualize plasma membrane, and mCit-MBD (pPDF1::mCit-MBD) line was used for visualization of MTs.

Confocal imaging of the cell outlines and image processing

The epidermal pavement cell outlines were imaged from the adaxial surfaces of 3-week-old *Arabidopsis thaliana* leaves. Small sections (5 mm^2) were sampled from the central part of the leaves and submerged in a staining solution of 0.1% Propidium Iodide (PI) (Sigma, Cat: 81845) dissolved in water for 20 minutes. After a brief rinse in water, the samples were mounted on a slide with a cover slip and imaged using a Leica TCS SP5 upright laser confocal microscope equipped with a water immersion objective (25x/0.95). The excitation and emission wavelength windows used were 488 nm and 600-650 nm for PI and 488 nm and 495-545 nm for GFP, respectively. The images were acquired with 1024x1024 resolution and z-stack slices with 0.5-1 µm in the z-direction. At least 10 different plants and leaves from the adaxial sides were collected at the same de-

velopmental stage for each genotype. The confocal images were processed in MorphoGraphX using *Gaussian Blur Stack* and *Brighten Darken* filters to enhance the clarity of cell outlines. The confocal signal was then projected onto a mesh, reconstructing the three-dimensional structure of the sample (2.5D). Cell segmentation was performed using seeding and *Watershed Segmentation* processes. Heatmaps for cell parameters including Lobeyness, Min Axis, Area, and LEC were generated using MorphoDynamX. Correlation analysis between contour parameters was conducted using the MDXtoR plugin.

Sampling of different plant species

The analysis of epidermal cell outlines from different species (see Suppl. Table 1) was conducted using specimens collected from commonly grown species in Cologne (Germany) and Norwich (United Kingdom). To obtain the cell outlines, we employed the imprinting method with 3% Low Melting Point (LMP) agarose (ROTH, Germany, Cat: 39346-81-1) dissolved in dH2O. The agarose solution was briefly microwaved until boiling and then allowed to cool to room temperature without solidifying. On a microscope slide, a droplet of the lukewarm agarose was carefully dispensed, small fragments (1 cm^2) were excised from the central region of the plant organs using a razor blade and then gently transferred onto the lukewarm agarose droplets and allowed to solidify. The plant sections were carefully removed from the slide while keeping the agarose intact, thus preserving the shape of the epidermal cells. The slides with the agarose imprints were subsequently stored at 4°C until they were imaged. Imprints were obtained from both the adaxial and abaxial sides of all collected organs, excluding green fruit, stamen, stigma, and bract. The identification of plant species was conducted using references such as Simpson (2006) and Harris and Harris (2001).

Phase-contrast microscopy of epidermal imprints

The transparent epidermal imprints, with a thickness of 5-10 µm, were visualized using either a Zeiss Axio Imager M2 microscope equipped with an Axiocam 512 camera, or a Nikon Microphot-SA microscope connected to a Leica camera. Air Plan-NEOFLUAR objectives of either x20 or x40 were utilized, depending on the cell size of the sample being imaged. To ensure representative coverage, each image typically contained approximately 50 cells, adjusted based on the specific sample. The phase-contrast mode was employed for imaging on both microscopes. The images were acquired using ZEN 2.3 software for the Zeiss Axio Imager M2 microscope, utilizing the tailing mode to stitch multiple images (5x5), or LAS software for the Nikon Microphot-SA microscope.

Image acquisition for Miocene plant species

The Miocene plant fossils analyzed in this study were obtained from datasets published by Reichgelt *et al.* (2020). These fossils were preserved in turbidite deposits within the Foulden Maar diatomite core. To prepare the fossilized leaves for analysis, they were treated with hydrogen peroxide and tetra-sodium pyrophosphate salt crystals. This treatment effectively removed mesophyll cell debris, ensuring clearer observation of the leaf structures. The cleaned fossil leaves were then stained with Crystal Violet and mounted on glass slides using glycerin jelly. High-resolution images of the leaves were captured at 100× magnification using TSView 7.1.1.2 microscope imaging software on a Nikon Optiphot microscope. Species identification of the fossil specimens was based on paleobotanical studies and comparison with known species from the Foulden Maar surface exposures.

Image processing for multispecies pavement cell outline analysis

To improve the visualization of cell outlines, GNU Image Manipulation Program (GIMP) was used to enhance saturation, contrast, and sharpness. Each image contained a maximum of 50 cells, and only cells with clear outlines were manually traced. Fiji software was used to calculate the distance in pixels along the scale length, which was used to calibrate the scale bars in MorphoGraphX (Strauss *et al.,* 2022). To aid in cell segmentation, various image filters, including *Invert*, *Gaussian Blur Stack*, and *Brighten Darken*, were applied. The surface mesh was extracted using the *Marching Cubes Surface* algorithm with a cube size of 5 µm. The cell outlines from the phase-contrast microscopy images were projected onto the mesh, and cell segmentation was achieved by applying the *Watershed Segmentation process*. To further refine the cell contours, the *Smooth Mesh* process was applied, resulting in a smoother and more accurate representation of the cells. The cell contours obtained from the segmented mesh were then analyzed and quantified using MorphoDynamX. A subset of the most representative cell contours was selected for further analysis, ensuring a focus on the cells that were most relevant to the research objectives. Heatmaps for Lobeyness, Min Axis, Area, and LEC were generated using the *Contour process*. Correlation analysis between two contour parameters was performed using the MDXtoR plugin.

Dose-dependent drug treatment

To investigate the effects of oryzalin or latrunculin B on *Arabidopsis thaliana* cotyledon pavement cells, plates containing 50 mL of MS medium (0.7% agar, without sugar and vitamins) were prepared. The drugs, oryzalin (Sigma-Aldrich, Cat: 36182) or latrunculin B (Sigma-Aldrich, Cat: L5288), were added to the plates at final concentrations of 0.5, 1, 5, 8, 10, 20, and 50 µM. As a control, DMSO (Dimethyl sulfoxide, Sigma, Cat: D8418) was added alone at an amount equivalent to the highest drug concentration. After 6 days, the cotyledons were collected and mounted on microscope slides with cover slips. Images of the cotyledon pavement cells were captured using the Zeiss Axio Imager M2 light microscope. The captured images were then processed to segment the cells and quantify their contours.

Osmotic treatments and turgor pressure study

To study the cell outlines of *Arabidopsis* wild type and pAR169 lines, 6-day-old cotyledons were dissected and stained with a 0.1% PI solution for 30 minutes. The cotyledons were then imaged using a Leica SP8 microscope equipped with a x25 water immersion objective. For fluorescence imaging, a 514nm laser excitation was used. The fluorescence signal was collected from 605nm to 642nm for PI and from 521nm to 551nm for mCit-MBD and pAR169. This allowed for the visualization of the respective signals in the cotyledon cells. Each cotyledon was imaged first in water to capture the initial state, and then again after 50 minutes in a sorbitol solution with a concentration of 0.6M.

For the turgor pressure study, cotyledons from the *Arabidopsis* wild type were dissected and imaged using a Nikon SMZ18 stereomicroscope with a x6 zoom. The cotyledons were placed between a curved microscope slide and a lamella, with drops of either water or NaCl solution. Pictures were taken after 15 minutes in NaCl solutions of increasing concentrations. The concentrations used were 0, 0.1, 0.15, 0.175, 0.2, 0.225, 0.25, 0.3, and 0.4 M. The specific concentrations were determined through osmometer measurements (Gonotec® Osmomat™ 030 cryoscopic osmometer), ensuring accurate control over the osmotic environment.

Growth quantification for epidermis of juvenile maize leaves

Maize (Zea mays cv. 'Polonez' and 'Cosmo') caryopses were kept submerged in water for 6 h, germinated on blotting paper for 18 h in light at room temperature, transferred to plastic containers filled with moist soil, and grown in glasshouse (temperature 19-21 °C, additional illumination to obtain 16 h day). After 4-7 days, a longitudinal strip of coleoptile or coleoptile and the first leaf sheath was gently removed to expose the base of the first or second juvenile leaf, respectively. The sequential replica method (Williams and Green, 1988; Kwiatkowska and Burian, 2014) was used to obtain silicon moulds, made of Take 1 Advanced Impression Material (Light Body Wash, Kerr Corp., Romulus, USA) from the abaxial epidermis of the exposed leaf epidermis surface. Two replicas were taken from each leaf at 24 h interval. After replica taking the exposed leaf portion was protected from drying by food wrap. Epoxy resin replicas (casts made from Devcon 2 Ton Clear epoxy) were obtained from the silicon moulds, sputter-coated and observed using scanning electron microscopy (Hitachi UHR FE-SEM SU8010). Pairs of stereoimages were taken from each region of interest and used for the stereoscopic reconstruction of the leaf surface (Routier-Kierzkowska and Kwiatkowska, 2008). Growth was analysed for 2 juvenile leaves of cv. 'Polonez' and 3 juvenile leaves of cv. 'Cosmo'. For each leaf, 3-12 patches of epidermis were identified in the two consecutive replicas, located at an increasing distance from the intercalary meristem. Because maize pavement cells become strongly elongated, in each patch, 3-9 groups (nearly square-shaped in the first replica), which comprised 6-12 adjacent cells, were used to compute areal growth rates and Principal Growth Directions (Dumais and Kwiatkowska, 2002).

Spring model

The mass-spring mechanical model was performed based on a published study by Sapala *et al.* (2018). Cell walls were delineated by point masses linked together by springs, which allowed to modify cell wall segment lengths and point mass positions to simulate the process of tissue growth. The model facilitated the introduction of additional intracellular connections that represent the deposition of microtubules within cells based on predefined conditions. Importantly, these connections are restricted to locations where physical constraints—such as visibility, proximity, and alignment to the cell wall—permit their formation. Three distinct growth patterns were incorporated into the simulation to demonstrate the dynamics of growth: uniform isotropic, uniform anisotropic, and non-uniform growth. Each growth pattern led to different forms of cell deformation, creating a dynamic simulation environment where the location of every point mass was continuously updated from one timestep to the next. The model was used to recreate the orientation and distribution of microtubules, which were observed through confocal imaging, based on the initial outlines of cell walls. In the simulation, the model begun with the cell wall outlines and assumed that microtubules reorganize in response to mechanical stress.

Author contribution:

Conceptualization: RSS, MM. **Methodology:** NT, RSS, MM. **Investigation:** NT, BL, AP, YW, LH, MA, CM, AM, TR, DK, RSS, MM. **Formal analysis:** NT, MA, FC, DK, AR, RSS, MM. **Data curation:** NT, AR, RSS, MM. **Writing – original draft:** RSS, MM, NT. **Writing – review & editing:** NT, AM, TR, OH, AB, DK, AR, RSS, MM. **Funding acquisition:** OH, AB, DK, RSS, MM. Supervision: AHKR, OH, AB, DK, RSS, MM.

Acknowledgement:

ERA-CAPS (CM, AB, DK, RSS, MM), John Innes Foundation (NT), EMBO Postdoctoral Fellowship (LH), NSF IOS 1553030 (AHKR). We acknowledge Dr. Izabela Potocka from the Electron Microscopy Laboratory of Institute of Biology, Biotechnology and Environmental Protection, University of Silesia for help in SEM of replicas. We thank Dr. Azahara Martin for providing us with access to the phase-contrast microscope. We would like to thank Prof. Geoffrey Wasteneys for providing *any1* seeds, and the Nottingham Arabidopsis Stock Center for distributing other seeds. The confocal microscopy was performed at the Cellular Imaging Facility (CIF), University of Lausanne.

References:

Baskin TI. Anisotropic expansion of the plant cell wall. Annu Rev Cell Dev Biol. 2005;21:203-22. doi: 10.1146/annurev.cellbio.20.082503.103053.

Beauzamy L, Nakayama N, Boudaoud A. Flowers under pressure: ins and outs of turgor regulation in development. Ann Bot. 2014 Nov;114(7):1517-33. doi: 10.1093/aob/mcu187.

Bidhendi AJ, Lampron O, Gosselin FP, Geitmann A. Microscale geometrical features in the plant leaf epidermis confer enhanced resistance to mechanical failure. bioRxiv 2022.12.10.519895; doi: https://doi.org/10.1101/2022.12.10.519895.

Bush RT, Wallace J, Currano ED, Jacobs BF, McInerney FA, Dunn RE, Tabor NJ. Cell anatomy and leaf δ13C as proxies for shading and canopy structure in a Miocene forest from Ethiopia, Palaeogeography, Palaeoclimatology, Palaeoecology, Volume 485, 2017, Pages 593-604, ISSN 0031-0182. doi.org/10.1016/j.palaeo.2017.07.015.

Carter R, Woolfenden H, Baillie A, Amsbury S, Carroll S, Healicon E, Sovatzoglou S, Braybrook S, Gray JE, Hobbs J, Morris RJ, Fleming AJ. Stomatal Opening Involves Polar, Not Radial, Stiffening Of Guard Cells. Curr Biol. 2017 Oct 9;27(19):2974-2983.e2. doi: 10.1016/j.cub.2017.08.006.

Dumais J, Kwiatkowska D. Analysis of surface growth in shoot apices. Plant J. 2002 Jul;31(2):229-41.

Elsner J, Lipowczan M, Kwiatkowska D. Differential growth of pavement cells of Arabidopsis thaliana leaf epidermis as revealed by microbead labeling. Am J Bot. 2018 Feb;105(2):257-265. doi: 10.1002/ajb2.1021.

Fu Y, Li H, Yang Z. The ROP2 GTPase controls the formation of cortical fine F-actin and the early phase of directional cell expansion during Arabidopsis organogenesis. Plant Cell. 2002 Apr;14(4):777-94. doi: 10.1105/tpc.001537.

Fujita M, Himmelspach R, Ward J, Whittington A, Hasenbein N, Liu C, Truong TT, Galway ME, Mansfield SD, Hocart CH, Wasteneys GO. The anisotropy1 D604N mutation in the Arabidopsis cellulose synthase1 catalytic domain reduces cell wall crystallinity and the velocity of cellulose synthase complexes. Plant Physiol. 2013 May;162(1):74-85. doi: 10.1104/pp.112.211565.

Gendreau E, Traas J, Desnos T, Grandjean O, Caboche M, Höfte H. Cellular basis of hypocotyl growth in Arabidopsis thaliana. Plant Physiol. 1997 May;114(1):295-305. doi: 10.1104/pp.114.1.295.

Glover BJ. Differentiation in plant epidermal cells. J Exp Bot. 2000 Mar;51(344):497-505. doi: 10.1093/jexbot/51.344.497.

Hülskamp M, Folkers U, Grini PE. Cell morphogenesis in Arabidopsis. Bioessays. 1998 Jan;20(1):20-9. doi: 10.1002/(SICI)1521-1878(199801)20:1.

Jacques E, Verbelen JP, Vissenberg K. Review on shape formation in epidermal pavement cells of the Arabidopsis leaf. Funct Plant Biol. 2014 Sep;41(9):914-921. doi: 10.1071/FP13338.

Kürschner WM. The anatomical diversity of recent and fossil leaves of the durmast oak (Quercus petraea Lieblein/Q. pseudo-castanaea Goeppert) — implications for their use as biosensors of palaeoatmospheric CO2 levels. Review of Palaeobotany and Palynology 1997 96(1–2): 1–30. doi.org/10.1016/S0034-6667(96)00051-6.

Kutschera U, Niklas KJ. The epidermal-growth-control theory of stem elongation: an old and a new perspective, Journal of Plant Physiology, 2007, vol. 164 (pg. 1395-1409).

Kwiatkowska D, Burian A. Sequential replicas for in vivo imaging of growing organ surfaces. Methods Mol Biol. 2014;1080:99-110. doi: 10.1007/978-1-62703-643-6_8.

Lee GY, Cheung K, Chang W, Lee LP (2000) Mechanical interlocking with precisely controlled nano- and microscale geometries for implantable microdevices. 1st Conference on Microtechnologies in Medicine and Biology. Proceedings (Cat. No.00EX451). doi: 10.1109/MMB.2000.893842.

Majda M, Grones P, Sintorn IM, Vain T, Milani P, Krupinski P, Zagórska-Marek B, Viotti C, Jönsson H, Mellerowicz EJ, Hamant O, Robert S. Mechanochemical Polarization of Contiguous Cell Walls Shapes Plant Pavement Cells. Dev Cell. 2017 Nov 6;43(3):290-304.e4. doi: 10.1016/j.devcel.2017.10.017.

Panteris E, Galatis B. The morphogenesis of lobed plant cells in the mesophyll and epidermis: organization and distinct roles of cortical microtubules and actin filaments. New Phytol. 2005 Sep;167(3):721-32. doi: 10.1111/j.1469-8137.2005.01464.x.

Panteris E, Apostolakos P, Galatis B. Sinuous ordinary epidermal cells: behind several patterns of waviness, a common morphogenetic mechanism. New Phytol. 1994 Aug;127(4):771-780. doi: 10.1111/j.1469-8137.1994.tb02981.x.

Reichgelt T, D'Andrea WJ, Valdivia-McCarthy AC, Fox BRS, Bannister JM, Conran JG, Lee WG, Lee DE. Elevated CO2, increased leaf-level productivity, and water-use efficiency during the early Miocene, Clim. Past, 16, 1509–1521, 2020. doi: 10.5194/cp-16-1509-2020.

Routier-Kierzkowska AL, Kwiatkowska D. New stereoscopic reconstruction protocol for scanning electron microscope images and its application to in vivo replicas of the shoot apical meristem. Funct Plant Biol. 2008 Dec;35(10):1034-1046. doi: 10.1071/FP08047. PMID: 32688852.

Sapala A, Runions A, Routier-Kierzkowska AL, Das Gupta M, Hong L, Hofhuis H, Verger S, Mosca G, Li CB, Hay A, Hamant O, Roeder AH, Tsiantis M, Prusinkiewicz P, Smith RS. Why plants make puzzle cells, and how their shape emerges. Elife. 2018 Feb 27;7:e32794. doi: 10.7554/eLife.32794.

Sampathkumar A, Krupinski P, Wightman R, Milani P, Berquand A, Boudaoud A, Hamant O, Jönsson H, Meyerowitz EM. Subcellular and supracellular mechanical stress prescribes cytoskeleton behavior in Arabidopsis cotyledon pavement cells. Elife. 2014 Apr 16;3:e01967. doi: 10.7554/eLife.01967.

Schwarz EM, Roeder AH. Transcriptomic Effects of the Cell Cycle Regulator LGO in Arabidopsis Sepals. Front Plant Sci. 2016 Nov 22;7:1744. doi: 10.3389/fpls.2016.01744.

Sotiriou P, Giannoutsou E, Panteris E, Galatis B, Apostolakos P. Local differentiation of cell wall matrix polysaccharides in sinuous pavement cells: its possible involvement in the flexibility of cell shape. Plant Biol (Stuttg). 2018 Mar;20(2):223-237. doi: 10.1111/plb.12681.

Strauss S, Runions A, Lane B, Eschweiler D, Bajpai N, Trozzi N, Routier-Kierzkowska AL, Yoshida S, Rodrigues da Silveira S, Vijayan A, Tofanelli R, Majda M, Echevin E, Le Gloanec C, Bertrand-Rakusova H, Adibi M, Schneitz K, Bassel GW, Kierzkowski D, Stegmaier J, Tsiantis M, Smith RS. Using positional information to provide context for biological image analysis with MorphoGraphX 2.0. Elife. 2022 May 5;11:e72601. doi: 10.7554/eLife.72601. PMID: 35510843; PMCID: PMC9159754.Vőfély RV, Gallagher J, Pisano GD, Bartlett M, Braybrook SA. Of puzzles and pavements: a quantitative exploration of leaf epidermal cell shape. New Phytol. 2019 Jan;221(1):540-552. doi: 10.1111/nph.15461.

Watson R.W. The effect of cuticular hardening on the form of epidermal cells. New Phytol., 41 (1942), pp. 223-229.

Williams MH, Green PB Sequential scanning electron microscopy of a growing plant meristem. Protoplasma 1988 147: 77–79.

Zuch DT, Doyle SM, Majda M, Smith RS, Robert S, Torii KU. Cell biology of the leaf epidermis: Fate specification, morphogenesis, and coordination. Plant Cell. 2022 Jan 20;34(1):209-227. doi: 10.1093/plcell/koab250.

Zhao X., Yang Y., Shen Z., Zhang H. H., Wang G., Gan Y. 2006. Stomatal clustering in *Cinnamomum camphora*. South African Journal of Botany 72 565 569.